J Appl Electrochem (2007) 37:1455–1462
DOI 10.1007/s10800-007-9361-x

ORIGINAL PAPER

Ruthenium selenide catalysts for cathodic oxygen reduction in direct methanol fuel cells

Alexander Racz · Petra Bele · Carsten Cremers · Ulrich Stimming

Received: 6 November 2006 / Revised: 25 June 2007 / Accepted: 30 June 2007 / Published online: 27 July 2007

Abstract The oxygen reduction reaction in sulphuric acid on commercial carbon supported platinum and ruthenium catalysts as well as on a home-made carbon supported ruthenium selenide catalysts ($RuSe_x$/C) was investigated. The $RuSe_x$/C catalysts were synthesised using similar procedures to those found in the literature. A dependency of H_2O_2 formation on the selenium content was found using the thin-film rotating ring disc electrode technique, namely that the H_2O_2 formation in the typical operation range of a Direct Methanol Fuel Cell (0.7–0.4 V) on Pt/C is below 1% and 1–4% on Ru/C and $RuSe_x$/C catalysts. Finally for comparing the intrinsic activities of the catalysts the electrochemically active surface areas were determined in-situ by means of copper underpotential deposition. Our results indicate a comparable activity of the present $RuSe_x$/C catalyst to commercial Pt/C if the activities are related to the electrochemical active areas.

Keywords Oxygen reduction · Rotating ring disc electrode · Copper underpotential deposition · Ruthenium · Selenium

A. Racz (✉) · P. Bele · U. Stimming
Department of Physics E19, TU München, James-Franck-Street 1, 85748 Garching, Germany
e-mail: aracz@ph.tum.de

C. Cremers · U. Stimming
Division 1, ZAE Bayern, Walther-Meißner Street 6, 85748 Garching, Germany

Present Address:
C. Cremers
Fraunhofer Institut Chemische Technologie (ICT), Joseph-von-Fraunhofer-Street 7, 76327 Pfinztal, Germany

1 Introduction

Direct Methanol Fuel Cells (DMFC) are a promising power source, especially for portable applications, having numerous advantages, e.g. the high energy density of methanol [1]. However, the performance of a DMFC is limited by a number of problems including (1) sluggish kinetics of the anodic methanol oxidation, (2) sluggish kinetics of the cathodic oxygen reduction reaction (ORR) and (3) methanol cross-over from the anode side to the cathode side, resulting in a mixed potential at non-selective Pt-based cathodes [2]. Up to now carbon-supported platinum is generally used as the cathode catalyst. But in order to avoid the formation of a mixed potential either novel membranes with much reduced methanol permeation have to be developed or methanol-tolerant catalysts have to be used at the cathode. Ruthenium modified with Selenium has proven to be a stable and highly selective catalyst towards the ORR in the presence of methanol [3, 4]. In earlier results of our group $RuSe_x$ nanoparticles were synthesized on a carbon support (Vulcan XC72), but the particles were coarse in nature and substantial agglomeration occurred [5]. The aim of this work was to further improve the dispersion of the catalyst and to yield a high electrochemical active area of $RuSe_x$/C catalysts. Therefore, the synthesis procedures described in the literature, e.g. [6], were modified as reported in our previous publication [7] and the so prepared home-made $RuSe_x$/C catalysts were electrochemically tested. Comparisons concerning the electrochemical activity with respect to the ORR to commercial Pt/C and Ru/C catalysts are made.

For a true comparison of different catalysts the intrinsic activities of the catalysts are important and therefore the real surface area, i.e. the electrochemically active area (ECA), has to be known. Thus in this study the electrochemical active

areas of all catalysts were determined by Cu underpotential deposition (Cu-UPD) and the intrinsic activities are compared.

2 Experimental details

Solutions were prepared from 98% H_2SO_4 (Merck) and deionized water (18 MΩ cm^{-1}, Millipore Milli-Q system). The 40 wt% Ru/C and 40 wt% Pt/C used were commercially available (ETEK).

2.1 Catalyst preparation

The 32 wt% $RuSe_x$/C as well as the 40 wt% $RuSe_x$/C catalyst were synthesised by thermolysis of a ruthenium precursor $Ru_3(CO)_{12}$ (Alfa Aesar) and elemental selenium powder (Alfa Aesar, 200 mesh) in *o*-xylene (Merck, b.p. ~142°C), which was dried using molecular sieves. The synthesis was carried out as described previously [7]. In short the selenium was dissolved under reflux conditions in dried *o*-xylene, $Ru_3(CO)_{12}$ and milled Vulcan XC72R together were ultrasonically dispersed in dried *o*-xylene and this dispersion was slowly added to the boiling Se-containing solution. After 20 h of synthesis under reflux conditions and vigorous stirring a black powder was obtained, which was filtered, washed with diethylether and dried in air.

2.2 Analytical techniques

2.2.1 Transmission electron microscopy analysis

One additional point in this work is to demonstrate a combination of advanced electron microscopy techniques that can be efficiently used to identify and characterize the individual catalysts. Therefore, we used different techniques including conventional bright-field TEM, energy-filtered TEM (EF-TEM), high-angle annular dark field scanning transmission electron microscopy (HAADF-STEM) and energy dispersive X-ray spectrometry (EDX). These techniques enable information on the size, size distribution, morphology, crystalline structure and elemental composition of individual nano-scale particles of the catalyst.

To obtain information about the mean particle diameter and particle distribution, conventional bright-field TEM imaging was used together with advanced image processing [8]. Measurements were carried out on a JEOL 2010 microscope with LaB_6 cathode working at 120 keV. A magnification of 150,000 was chosen for all images involved in the data analysis and the focus was set around the Scherzer defocus of the microscope to receive the best point resolution. This setting ensures that one can always directly compare images and results for different samples. An additional point is that it makes the image processing faster due to the fact that the new advanced image processing can be used on a more or less basic set-up routine.

To efficiently characterize the metal composition of the catalysts EF-TEM and HAADF-STEM were used and the detailed identification of the composition was achieved through EDX measurements on single particles.

Whereas bright-field TEM images were formed by phase contrast, the HAADF detector detects electrons that are scattered to higher angles and almost only incoherent Rutherford scattering contributes to the image. Thereby, *Z*-contrast is achieved. The strong Coulomb interaction of the electrons with the potential of the atom core, which leads to high angle scattering (designated as Rutherford scattering), is employed by *Z*-contrast imaging in STEM mode. By this method, small clusters (or even single atoms) of heavy atoms can be imaged in a matrix of light atoms since the contrast is proportional to Z^2 (*Z*: atomic number).

In addition, the contrast in HAADF-STEM is focus independent, due to the above mentioned fact that the image is formed by incoherent scattering.

The dark-field measurements were preformed at a TECNAI G2 F20 microscope with a 200 keV FEG (field emission gun). In this mode it was also possible to perform EDX measurements on single nanoparticles using an additional EDX detector.

2.3 Electrochemical techniques

2.3.1 Rotating ring disc electrode measurements

The electrochemical activities and the H_2O_2 formation of the home-made $RuSe_x$/C catalysts as well as a commercial 40 wt% Ru/C and 40 wt% Pt/C catalyst were measured using the thin-film rotating ring disc electrode (RRDE) technique [8]. The experiments were carried out in 0.5 M H_2SO_4 under continuous Ar-purging using a home-made glass cell with a three electrode setup. Potentials were determined using a Hg/Hg_2SO_4/0.5 M H_2SO_4 reference electrode connected to the cell through a Luggin capillary. However, all potentials in this paper are referred to the normal hydrogen electrode (NHE). RRDE measurements were performed at room temperature using a rotating Au disc/Pt ring electrode tip (Pine Instruments), Autolab PGSTAT 30 potentiostat and an analytical rotator with speed control (AFMSRX from Pine Instruments).

Thin catalyst layers were prepared by depositing the catalyst on the freshly polished Au disc. A suspension of the catalyst powder in a 0.05 wt% Nafion/ethanol mixture was obtained by ultrasonification of about 15 min. An

aliquot of the suspension was pipetted on the Au substrate, leading to a catalyst loading of 177 μg cm^{-2}. After evaporating the ethanol in air the electrode was carefully rinsed with deionized water and used for experiments.

2.3.2 Determination of the electrochemical active area

A conventional glass cell with a three electrode setup, namely a polished glassy carbon (GC) working electrode (7 mm diameter, 0.385 cm^2 geometric surface area) which served as a substrate for the powder catalysts, a Pt sheet as counter electrode and a $Hg/Hg_2SO_4/0.5$ M H_2SO_4 reference electrode, was used to determine the electrochemical active area of the catalysts. All potentials refer to NHE. A PGSTAT 20 from Autolab was used as potentiostat. The catalyst layer preparation and the catalyst loading on the GC substrate were the same as described in Sect. "Rotating ring disc electrode measurements". Surface area measurements were carried out under continuous Ar-purging in 0.5 M H_2SO_4 and 0.5 M H_2SO_4 with 2 mM $CuSO_4$ (Merck) respectively.

3 Results

3.1 Structural characterization

3.1.1 Commercial 40 wt% Ru/C and 40 wt% Pt/C catalysts

The precise characterization and evaluation of carbon-supported catalysts using TEM is problematic due to the sample/support material and the imaging procedure itself [9]. The support material with its local thickness change results in a variation of the image contrast. In terms of the image detection it is possible that similar particles can appear with different intensities in the images, based on the diffraction contrast. An additional difficulty is to distinguish particles in the sub-nanometer scale from the matrix, due to the weak signal-to-noise ratio. Also an overlap between different particles can occur when imaged in projection. This leads to difficulties in distinguishing nanometer particles correctly from the matrix in some areas of the image. Therefore, we developed an advanced image processing routine to overcome those problems and to receive a reliable and reproducible characterization of the catalyst [9].

Figure 1 shows a typical TEM image of the commercial 40 wt% Pt/C catalyst. A non-homogeneous particle distribution is observed. Due to the high loading of platinum and/or the synthesis procedure large agglomerations of nanoparticles occur making a reliable analysis of the particle size and a calculation of the geometric particle surface area very difficult.

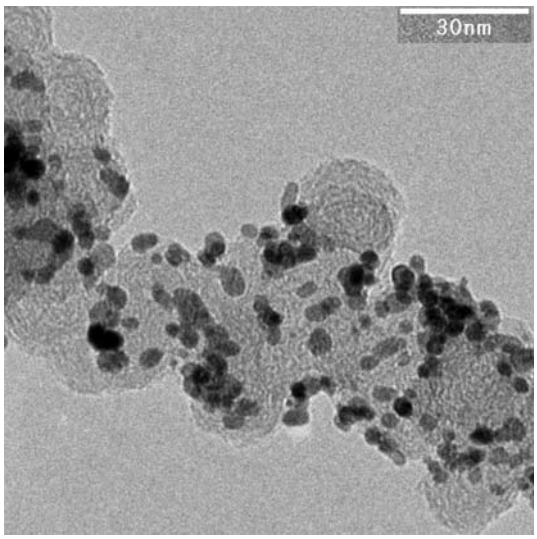

Fig. 1 Transmission electron microscopy bright-field image (raw data) taken at 120 keV of a commercial 40 wt% Pt/C (ETEK)

The same is true for Ru/C; a typical TEM image is shown in Fig. 2. The lower atomic number of Ru compared to Pt decreases the signal-to-noise ratio, which makes the distinction between small nanoparticles and the background with standard image processing even more difficult.

3.1.2 32 wt% $RuSe_x$/C and 40 wt% $RuSe_x$/C synthesised in xylene

Typical TEM images of Ru(26 wt%)Se(13 wt%)/C were already published in a previous publication (cf. Fig. 2 in Ref. [7]). The Ru(26 wt%)Se(6 wt%)/C (xyl) catalyst was investigated using conventional bright-field TEM and

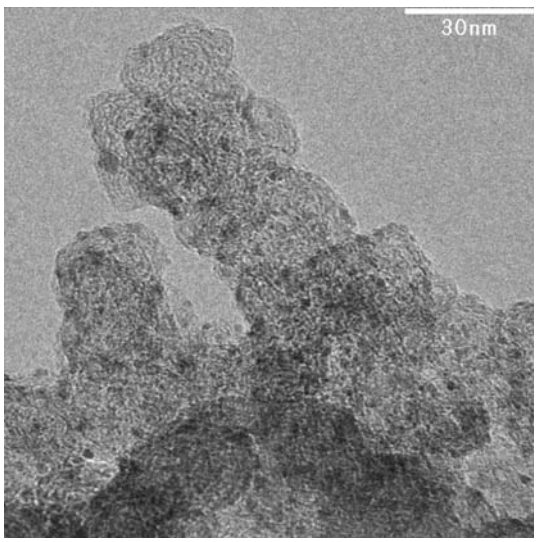

Fig. 2 Transmission electron microscopy bright-field image (raw data) taken at 120 keV of a commercial 40 wt% Ru/C (ETEK)

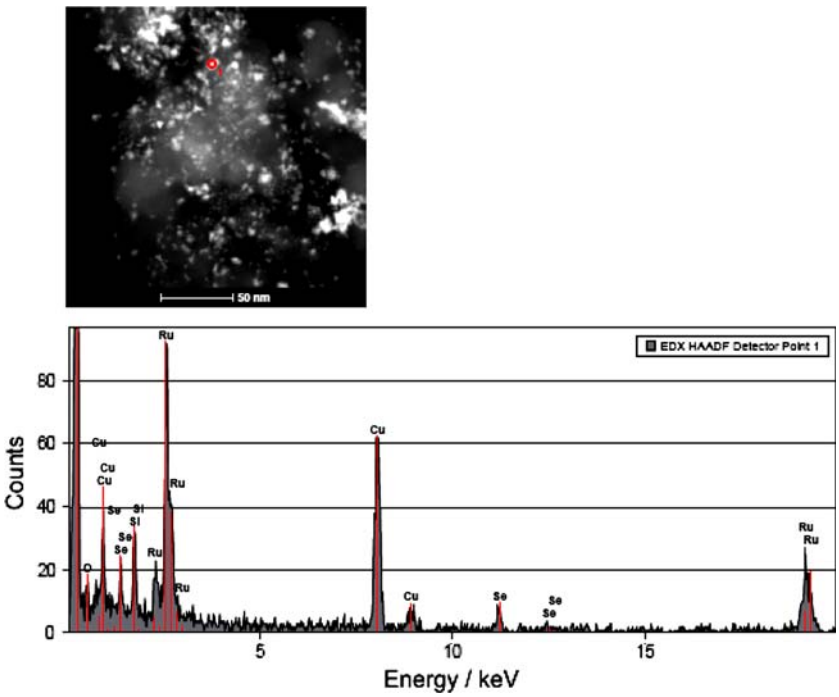

Fig. 3 High-angle annular dark field STEM image of a home-made Ru(26 wt%)Se(6 wt%)/C catalyst, synthesised in *o*-xylene. Image was taken with 200 keV. Below the corresponding EDX spectrum of the marked particle (*red cycle*) is depicted

HAADF-STEM measurements. Figure 3 shows a typical image taken at high magnification (450 k). The catalyst particles can be distinguished easily, but there is still some image contrast from the support material visible. This image contrast is due to the multiple scattering of the electrons in the thicker areas of the support material. The technique also allowed analysis of the composition of small particles using the EDX measurement (EDAX detector). Measurements were performed on a single particle (<10 nm) as shown in Fig. 3. The EDX data showed that the lower amount of selenium used in the synthesis resulted in ruthenium-rich nanoparticles, e.g. "$Ru_{7,5}Se$."

3.2 Electrochemical characterization

3.2.1 Collection efficiency

The electrochemical activity and the pathway of the ORR, i.e. the relative formation rates of H_2O (four electron pathway) and H_2O_2 (two electron pathway), can be determined using the thin-film RRDE technique. First, in order to calculate the fraction of H_2O_2 formation, the collection efficiency N has to be known, where N is defined as [10]:

$$N = -\frac{I_R}{I_D} \tag{1}$$

where I_R denotes the ring current and I_D is the disc current. This was done using the thin-film RRDE with a loading of 177 μg cm^{-2} Ru(26 wt%)Se(6 wt%)/C on the Au disc, prepared as described above. The electrolyte was deaerated 0.1 M NaOH with 10 mM $K_3[Fe(CN)_6]$. A Ag/AgCl/$KCl_{sat.}$ reference electrode was used. The measurements were performed at room temperature at a sweep rate v = 20 mV s^{-1}. Within the potential range investigated the collection efficiency N was N = 0.22, in exact agreement with the manufacturer's data (Pine Instruments). Furthermore the collection efficiency N was found to be independent of rotation rate (up to 2,500 rpm), (see Fig. 4).

Thus the fraction of H_2O_2 formation $(X_{H_2O_2})$ can be calculated [11]:

$$X_{H_2O_2} = \frac{2\,I_R/N}{I_D + I_R/N} \tag{2}$$

3.2.2 Oxygen reduction reaction

Figure 5a shows the oxygen reduction current densities, related to the geometric area of the electrode, in the positive and negative sweep for the 40 wt% Pt/C at room temperature in oxygen saturated 0.5 M H_2SO_4. Below 0.6 V a diffusion limited current for all rotation rates is observed. In the region between 0.6 V and the open circuit voltage (OCV, 1 V vs. NHE) the ORR is under mixed kinetic-diffusion control, similar to other results on carbon-supported Pt catalysts. Figure 5b shows the simultaneously recorded ring currents at 2,500 rpm. The ring was held at a constant potential of 1.24 V NHE, i.e. the region where the oxidation of H_2O_2 is diffusion limited. The ring currents are negligible in the region above 0.6 V, but increase significantly below 0.2 V due to adsorption of a hydrogen layer, which blocks sites for oxygen dissociation [11].

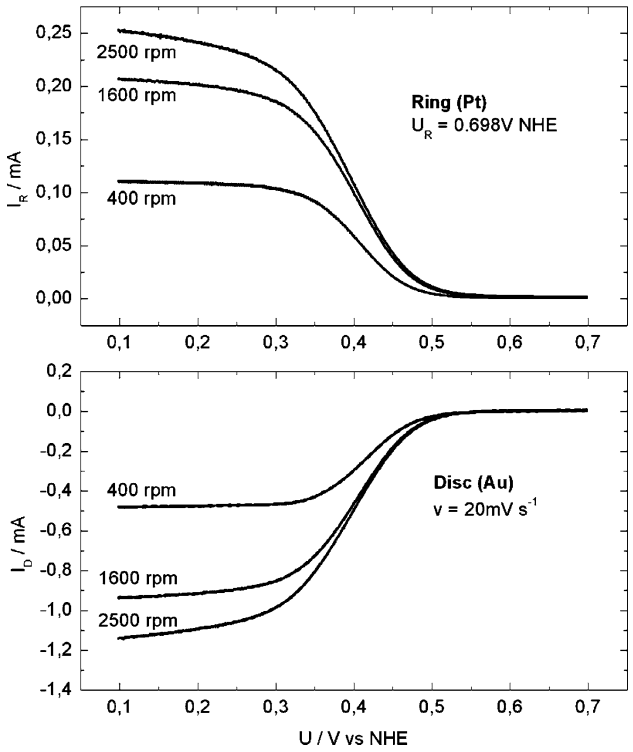

Fig. 4 Disc current i_D and ring current I_R on a 177 μg cm^{-2} $RuSe_x$/C catalyst thin-film RRDE in 0.1 M NaOH with 10 mM $K_3[Fe(CN)_6]$ at room temperature, sweep rate v = 20 mV s^{-1}, ring potential U_R = 0.698 V

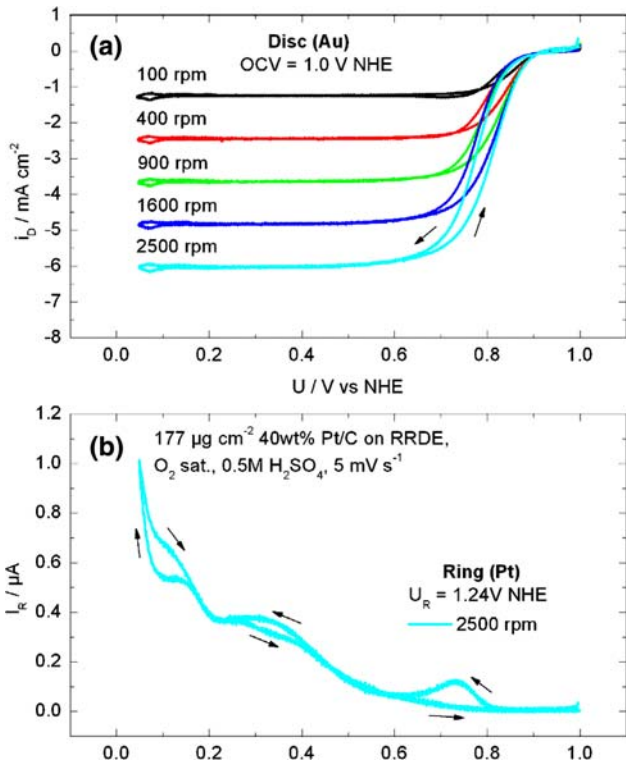

Fig. 5 Disc (i_D) and ring (I_R) currents during the oxygen reduction reaction on a 177 μg cm^{-2} 40 wt% Pt/C catalyst thin-film RRDE in oxygen saturated 0.5 M H_2SO_4 at a sweep rate of 5 mV s^{-1} at different rotation rates as indicated. Collection efficiency N = 0.22, ring potential U_R = 1.24 V, ring currents recorded at 2,500 rpm

Comparing the commercial Pt/C catalyst under the same conditions with the home-made $RuSe_x$/C catalyst, the OCV is about 150 mV lower on $RuSe_x$/C, (see Fig. 6a). However, below ca. 0.4 V a well defined diffusion limited current is observed. Figure 7b shows the ring currents at a rotation rate of 2500 rpm. This current is roughly one order of magnitude higher than on Pt/C.

The kinetic currents i_K were extracted using Koutecky-Levich plots by extrapolating to infinite rotation rate [10]. The calculated mass transport corrected currents for the positive and negative sweep were related to the mass of noble metal used and plotted vs. potential on a Tafel plot (Fig. 7). For clarity the commercial Ru/C and Pt/C, as well as the electrochemically most active home-made $RuSe_x$/C catalyst is shown. The $RuSe_x$/C catalyst has an overpotential approximately 100 mV higher than the Pt/C catalyst, but exhibits a higher activity than the Ru/C catalyst.

3.2.3 *Influence of selenium on the pathway of the oxygen reduction reaction*

Using Eq. (2) the fraction of H_2O_2 formation $(X_{H_2O_2})$ during the ORR can be calculated. The data were calculated from the RRDE measurements performed at 2,500 rpm in the positive sweep at four potentials in the typical operating range of a DMFC (0.7–0.4 V). A plot of the fraction of H_2O_2 formation as a function of selenium content of the ruthenium-based catalysts is shown in Fig. 8. Obviously the H_2O_2 formation depends on the Se content. The (Se-free) Pt/C and Ru/C catalysts are included as references. In this potential range the H_2O_2 formation on the Pt/C catalyst is negligible (below 1%), whereas on the Ru-based catalysts about 2–4% H_2O_2 are formed, similar to findings in [12].

3.2.4 *Determination of the electrochemical active surface area*

In order to compare the intrinsic activities of carbon-supported catalysts the ECA have to be known. For (carbon-supported) platinum and other platinum group metals like Ir and Rh the standard in-situ method is to use hydrogen adsorption [13], since on those surfaces hydrogen is adsorbed by UPD and the charge for adsorption (and likewise desorption) in this region is used to calculate the real surface area. However, on ruthenium the hydrogen adsorption method is not suitable because of (1) the overlap between regions of hydrogen adsorption and surface oxide reduction and (2) the overlap between hydrogen desorption

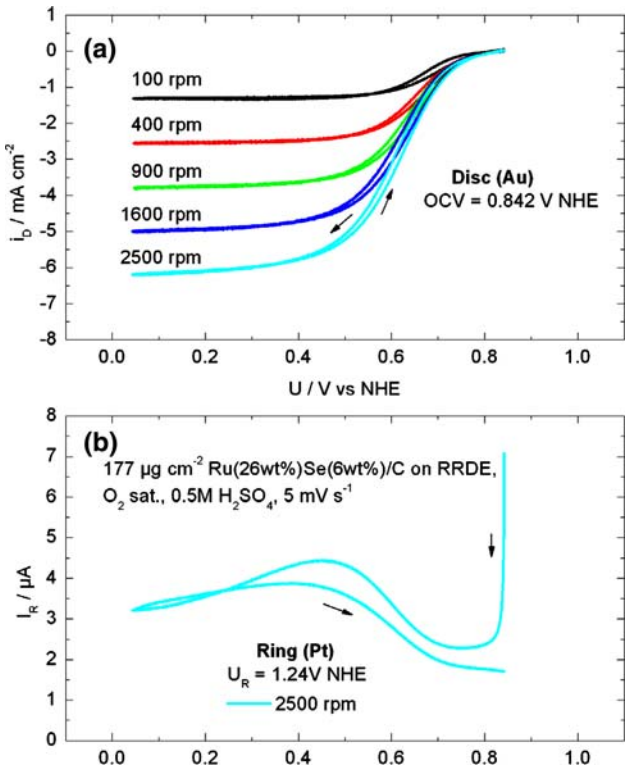

Fig. 6 Disc (i_D) and ring (I_R) currents during the oxygen reduction reaction on a 177 µg cm^{-2} Ru(26 wt%)Se(6 wt%)/C catalyst thin-film RRDE in oxygen saturated 0.5 M H_2SO_4 at a sweep rate of 5 mV s^{-1} at different rotation rates as indicated. Collection efficiency $N = 0.22$, ring potential $U_R = 1.24$ V, ring currents recorded at 2,500 rpm

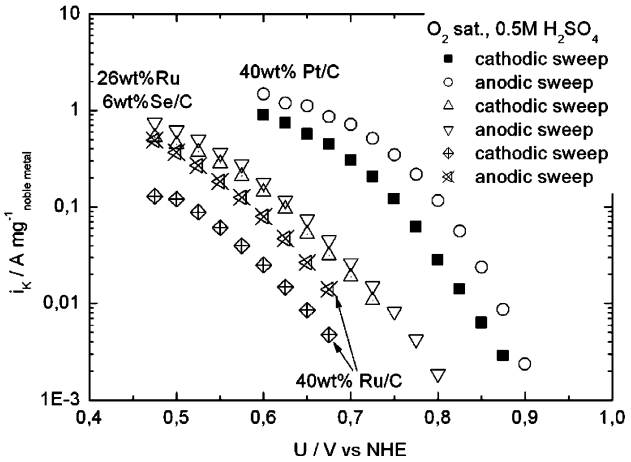

Fig. 7 Mass transport corrected mass-specific current densities for the oxygen reduction reaction at room temperature in oxygen saturated 0.5 M H_2SO_4 for three catalysts as indicated, obtained from the positive and negative sweeps

and ruthenium oxide formation and (3) absorption of hydrogen in the metal [14]. Thus, another technique to determine the real surface area of (carbon-supported)

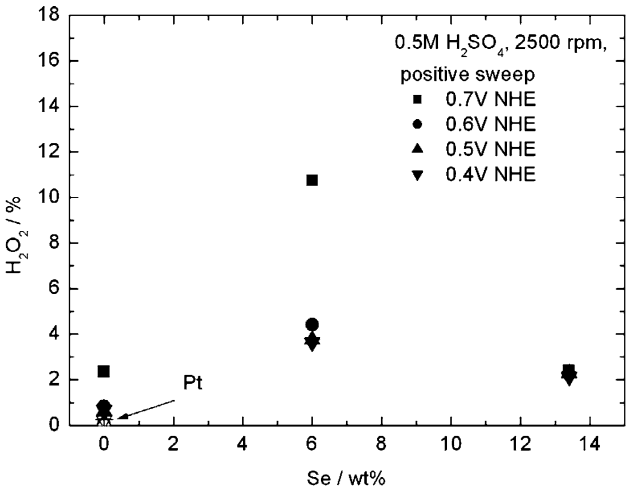

Fig. 8 Dependency of the H_2O_2 formation (%) on Se content (wt%) for Ru-based catalysts during oxygen reduction reaction in 0.5 M H_2SO_4 saturated with O_2. Pt/C is included as reference. The data was calculated from the positive sweeps at various potentials as indicated using Eq. 2

Ru-based catalysts has to be applied; a suitable one is the Cu-UPD [15]. With the assumption of an adsorption ratio of one Cu^{2+} ion to one surface metal atom, the UPD stripping charge ($Q_{Cu\text{-}UPD}$, 420 μC cm^{-2}) allows calculating the electrochemically available surface area. For this in-situ surface area determination an optimised deposition potential U_{dep} is required so that (1) no Cu is deposited either on the substrate (GC) or on the carbon support (Vulcan) and (2) only one monolayer of Cu is deposited on the electrochemical active sites, i.e. no bulk formation of copper. In a series of experiments with a thin film of Vulcan deposited on the GC substrate we found a deposition potential

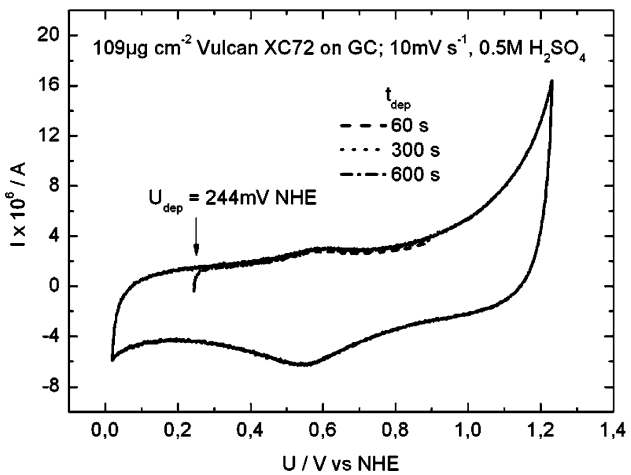

Fig. 9 Background and Cu-UPD stripping voltammograms of 109 µg cm^{-2} Vulcan XC72 thin-film on glassy carbon, sweep rate $v = 10$ mV s^{-1}. Copper deposition potential $U_{dep} = 244$ mV, deposition time t_{dep} as indicated

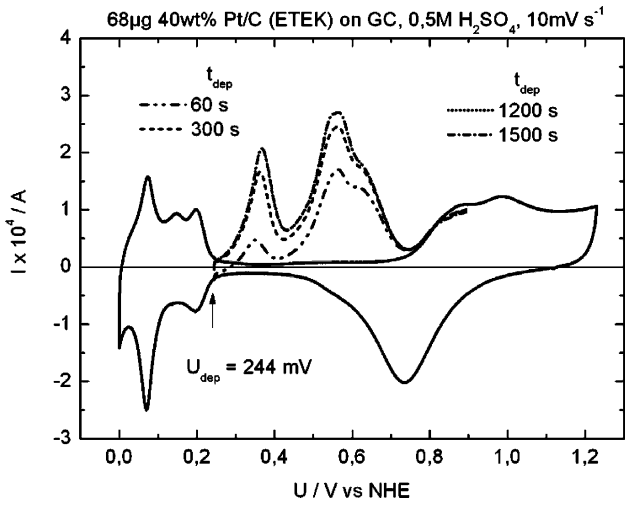

Fig. 10 Background and Cu-UPD stripping voltammograms of 177 µg cm^{-2} 40 wt% Pt/C catalyst thin-film on glassy carbon, sweep rate v = 10 mV s^{-1}. Copper deposition potential U_{dep} = 244 mV, deposition time t_{dep} as indicated

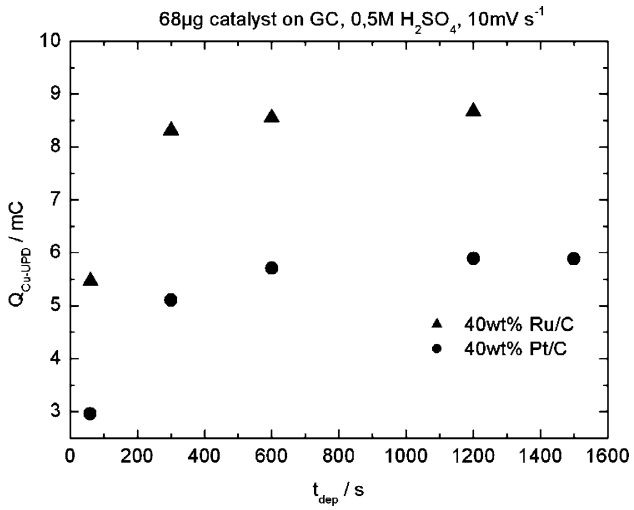

Fig. 12 Cu-UPD stripping charge ($Q_{Cu\text{-}UPD}$) for 40 wt% Ru/C and 40 wt% Pt/C in 0.5 M H_2SO_4 as a function of deposition time (t_{dep}). A saturation coverage is reached after 20 min which reflects the true active area

U_{dep} = 244 mV NHE, which fulfils the above mentioned first requirement, (see Fig. 9).

Figure 10 shows the determination of the active area of a commercial 40 wt% Pt/C catalyst using the Cu-UPD technique. The background voltammogram was recorded in deaerated 0.5 M H_2SO_4 at a sweep rate of 10 mV s^{-1} (black line). The stripping voltammograms were recorded in deaerated 0.5 M H_2SO_4 with 2 mM $CuSO_4$ after holding the potential at U_{dep} = 244 mV NHE for a certain time t_{dep} followed by a linear potential sweep from U_{dep} to 0.9 V NHE at 10 mV s^{-1}. Similarly the active area of Ru/C was determined as shown in Fig. 11.

The electrochemical active area was calculated for both catalysts by integrating the area between the stripping and the background voltammogram. By varying the deposition time t_{dep} a saturation effect is observed in both cases after t_{dep} = 20 min, confirming that no bulk deposition of copper occurred (see Fig. 12).

The same procedure was used to determine the electrochemical active area of the Ru(26 wt%)Se(6 wt%)/C catalyst, and again a saturation coverage is reached after 20 min. Therefore, the kinetic currents can be normalized to the active surface area and plotted as a function of the potential as shown in Fig. 13. This results, in comparison

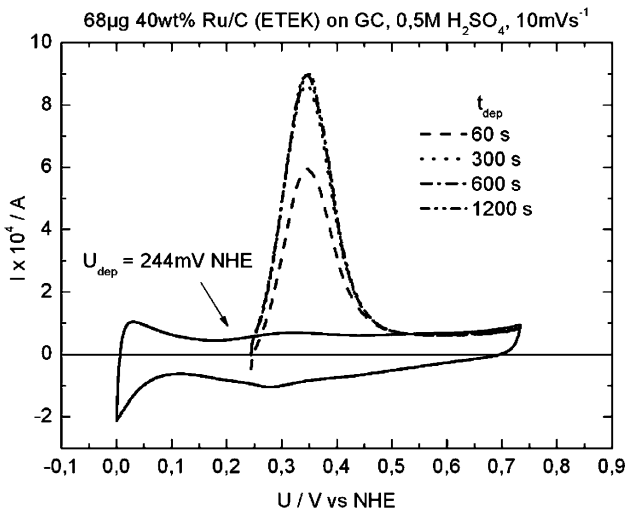

Fig. 11 Background and Cu-UPD stripping voltammograms of 177 µg cm^{-2} 40 wt% Ru/C catalyst thin-film on glassy carbon, sweep rate v = 10 mV s^{-1}. Copper deposition potential U_{dep} = 244 mV, deposition time t_{dep} as indicated

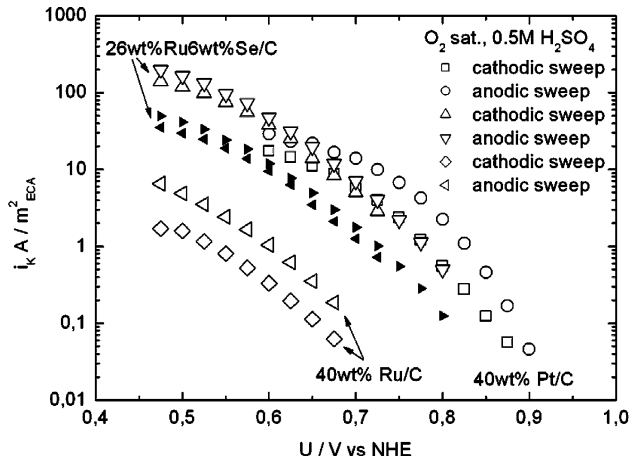

Fig. 13 Active surface area-normalized kinetic current densities for the oxygen reduction reaction at room temperature in oxygen saturated 0.5 M H_2SO_4 for three catalysts as indicated, obtained from the positive and negative sweeps. The *black triangles* indicate the lower limit of the active surface area-normalized activity of $RuSe_x/C$ (see text)

to the mass-related activity (see Fig. 7), in a large increase in the electrochemical activity of the $RuSe_x$/C catalyst, exhibiting a comparable performance to Pt/C and a superior performance to a Se-free Ru/C catalyst.

However, due to the formation of Cu_xSe [16] the stripping charge of 420 μC cm^{-2} does not correctly reflect the real surface area [17]. Since the Se surface composition of the catalyst is unknown so far our preliminary calculations (by using 420 μC cm^{-2} as the stripping charge) indicate that the active area of the $RuSe_x$/C catalyst is roughly an order of magnitude lower compared to Pt/C. However, if the catalyst surface is saturated with Se then the minimum value of 105 μC cm^{-2} might be used as discussed in [17]. This would mean that the surface area is underestimated and the maximum error in the surface area calculation is a factor of four. Consequently, the surface area-normalized activity of $RuSe_x$/C will be lowered by a factor of four at most (see black triangles for cathodic and anodic sweep in Fig. 12). But since this is considered to be the lower limit of the active surface area-normalized activity of $RuSe_x$/C and the true stripping charge will probably lie somewhere between 105 and 420 μC cm^{-2} $RuSe_x$/C may be regarded as an adequate alternative to Pt/C. A further increase in activity of $RuSe_x$/C may be achieved by even higher particle dispersion and lower peroxide formation. In order to better quantify the electrochemical active surface area (ECA), experiments with CO-Stripping on $RuSe_x$/C are planned. Due to the large anion contribution in the Faradic currents, we intend to perform DEMS (differential electrochemical mass spectrometry) experiments, similar to [17]. The relation of the Cu-UPD charge on a smooth surface studied in [17] may not be absolutely comparable to that of our nanoscopic $RuSe_x$/C particles.

Furthermore, it should be noted that the active areas were determined at a potential of 244 mV, a range where the majority of the ruthenium is reduced [15], and thus the active area may change at higher potentials due to the formation of oxides.

4 Conclusions

Home-made $RuSe_x$/C and commercial Ru/C and Pt/C catalysts were investigated and compared. Structural analysis via TEM and electrochemical characterisation via RRDE of the catalysts were performed. Due to agglomeration of nanoparticles a reliable analysis of the particle size and a calculation of the geometric particle surface area was not feasible.

It was possible to estimate the ECA of the catalysts by copper UPD deposition and the results indicate comparable activity of $RuSe_x$/C to Pt/C towards oxygen reduction in 0.5 M H_2SO_4 if the activities are related to the electrochemical active areas. It seems fact that the lower mass specific activity is due to a small active surface area of the $RuSe_x$/C. However, the relatively large peroxide yields of up to 4% on $RuSe_x$/C is a drawback which has to be overcome.

Acknowledgements We thank the BMBF for financial support under contract 01SF0302 ("O2RedNet") and the "Gemeinschaftslabor für Elektronenmikroskopie" (Prof. J. Mayer, RWTH Aachen) for use of their TECNAI G2 F20 microscope to perform the HAADF-STEM and EDX measurements. We also thank Dr Rainer Bußar for helpful discussions.

References

1. Arico AS, Srinivasan S, Antonucci V (2001) Fuel Cells 1:133
2. Ravikumar MK, Shukla AK (1996) J Electrochem Soc 143:2601
3. Alonso-Vante N, Bogdanoff P, Tributsch H (2000) J Catal 190:240
4. Solorza-Feria O, Ellmer K, Giersig M, Alonso-Vante N (1994) Electrochimica Acta 39:1647
5. Neergat M, Leveratto D, Stimming U (2002) Fuel Cells 2:25
6. Le Rhun V, Garnier E, Pronier S, Alonso-Vante N (2000) Electrochem Commun 2:475
7. Cremers C, Scholz M, Seliger W, Racz A, Knechtel W, Rittmayr J, Grafwallner F, Peller H, Stimming U (2007) Fuel Cells 7:21
8. Schmidt TJ, Gasteiger HA, Stab GD, Urban PM, Kolb DM, Behm RJ, (1998) J Electrochem Soc 145:2354
9. Bele P, Jäger F, Stimming U (2007) Microscopy and analysis (in press)
10. Bard AJ, Faulkner LR (2001) Electrochemical methods—fundamentals and applications, 2nd edn. Wiley, New York
11. Paulus UA, Schmidt TJ, Gasteiger HA, Behm RJ (2001) J Electroanal Chem 495:134
12. Schmidt TJ , Paulus UA, Gasteiger HA, Alonso-Vante N, Behm RJ (2000) J Electrochem Soc 147:2620
13. Biegler T, Rand DAJ, Woods R (1971) J Electroanal Chem 29:269
14. Hadzi-Jordanov S, Angerstein-Kozlowska H, Vukovic M, Conway BE (1977) J Phys Chem 81:2271
15. Green CL, Kucernak A (2002) J Phys Chem B 106:1036
16. Carbonnelle P, Lamberts L (1992) J Electroanal Chem 340:53
17. Nagel T, Bogolowski N, Baltruschat H (2006) J Appl Electrochem 36:1297